ELSEVIER

Rotation mechanism of shear fracture induced by high plasticity in Ti-based nano-structured composites containing ductile dendrites

Z.F. Zhang [a,*], G. He [b], H. Zhang [a], J. Eckert [c]

[a] *Shenyang National Laboratory for Materials Science, Institute of Metal Research, Chinese Academy of Sciences, 72 Wenhua Road, Shenhe District, Shenyang 110016, China*
[b] *Light Materials Group, National Institute for Materials Science, 1-2-1 Sengen, Tsukuba, Ibaraki 305-0047, Japan*
[c] *Physical Metallurgy Division, Department of Materials and Geo Sciences, Darmstadt University of Technology, Petersenstr. 23, D-64287 Darmstadt, Germany*

Abstract

Ti-based nano-structured composites with ductile dendrites often fail under a shear fracture angle larger than 45° with the compression stress axis. This can be explained by a rotation mechanism of the shear plane and bending of the shear bands, indicating a good mechanical performance of the nano-structured composites.
© 2004 Acta Materialia Inc. Published by Elsevier Ltd. All rights reserved.

1. Introduction

Bulk metallic glassy (BMG) materials have become a hot topic in the field of advanced materials due to the milestone discovery of Zr-based BMGs [1,2]. However, BMGs only exhibit high strength but, unfortunately, nearly zero plasticity, limiting their application as structural materials [3,4]. Recently, a major breakthrough in enhancing plasticity was achieved for BMG/nano-structured composites containing *in situ* precipitated dendritic phases upon solidification in Zr- and Ti-based alloys [5–10]. This improvement in plastic deformation is due to the strong blocking effect of the dendrites on the propagation of shear bands [5]. Normally, the shear band pattern formation into regular arrays was controlled by the ductile dendrites [5–8]. This opens the possibility of producing an entirely new class of high strength, tough, impact

and fatigue resistant materials, which combine the high strength of metallic glass with the ability to undergo plastic deformation under unconfined or otherwise unstable loading conditions [5]. Furthermore, there is the possibility of employing the newly developed BMG/nano-structured composites in many potential applications, such as biomaterials [10]. However, the basic deformation, fracture mechanisms and the high plasticity of the nano-structured Ti-based composites with ductile dendrites have not been systematically investigated so far. The main subject of the present paper is to reveal the details of the deformation and fracture mechanisms, and the plasticity under compressive loading, in order to better understand the properties of the newly developed nano-structured Ti-based composites [7–10].

2. Experimental procedures

The nano-structured matrix–dendrite composites, $(Ti_{40}Cu_{28}Ni_{24}Sn_8)_{1-x} (Ti_{80}Nb_{20})_x$, where x is equal to

* Corresponding author. Tel.: +86 24 23971043; fax: +86 24 23891320.
E-mail address: zhfzhang@imr.ac.cn (Z.F. Zhang).

Table 1
Compositions and shear fracture angles of the alloys A, B, C and D

Compositions of samples	Plastic strain (ε_P) (%)	Shear angle (θ_C^F) (°)	Shear angle (θ_C^0) (°)	($\theta_C^F - \theta_C^0$) (°)
A: $Ti_{56}Cu_{16.8}Ni_{14.4}Sn_{4.8}Nb_8$	8.9	46	43.5	2.5
B: $Ti_{60}Cu_{14}Ni_{12}Sn_4Nb_{10}$	21	48	41.4	6.6
C: $Ti_{64}Cu_{11.2}Ni_{9.6}Sn_{3.2}Nb_{12}$	24	50	41.9	8.1
D: $Ti_{66}Cu_8Ni_{4.8}Sn_{7.2}Nb_{14}$	30	51	40.5	10.5

0.4, 0.5 and 0.6, were fabricated by arc-melting. In addition, an alloy with an approximate composition of $Ti_{66}Cu_8Ni_{4.8}Sn_{7.2}Nb_{14}$ was selected. The compositions of the four alloys are listed in Table 1 and will be hereafter named as A, B, C and D alloys, respectively. The details of the fabrication processes of the nano-structured Ti-based composites have already been described elsewhere [9]. The characterization of the microstructure and the phases was done using a JEOL-JSM6400 scanning electron microscope (SEM). It was found that alloy A contains a relatively fine dendritic phase with a volume fraction of about 20%. For alloys B and C, the volume fractions of the dendrites are about 40% and 60%, respectively. Alloy D consists almost only of dendrites (about 95 vol.%) [9]. Normally, the distributions of the dendrites and the matrix are basically homogenous in the center of the samples. However, near the two surface layers of the samples, the dendrites are relatively fine in comparison with the other parts of the samples. Therefore, all the compressive specimens were cut into a dimension of $3\,mm \times 3\,mm \times 6\,mm$ from the middle parts of the alloys. Before the tests, they were mechanically polished, and then polished either by chemical or electrolytic methods. The compression tests were conducted with an Instron 8562 testing machine at room temperature under quasi-static loading conditions (strain rate of $10^{-4}\,s^{-1}$). After deformation or failure, all the specimens were investigated by SEM to reveal the deformation and fracture features.

3. Results and discussion

Fig. 1(a)–(d) show the compressive stress–strain curves and fracture morphologies of the alloys A–D. The four Ti-based alloys display typical initial elastic
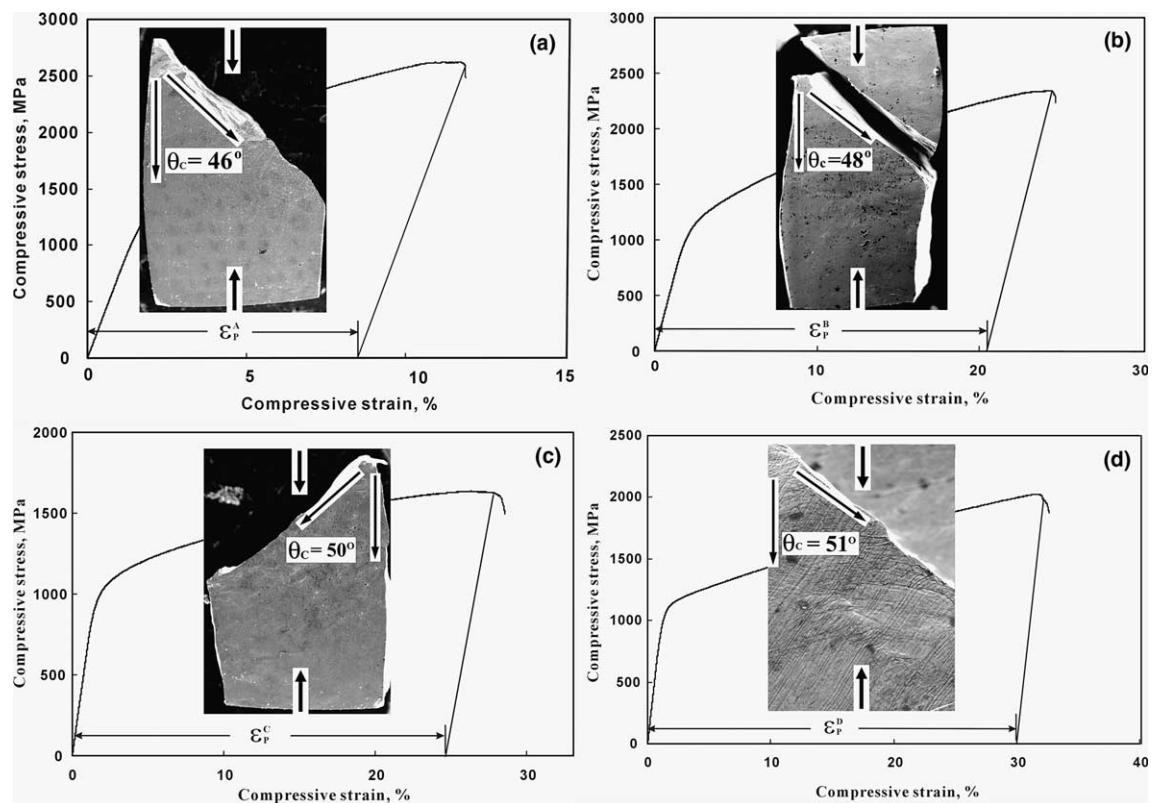
Fig. 1. Compressive stress-strain curves, fracture morphologies and shear fracture angles of the alloys A-D (a) alloy A; (b) alloy B; (c) alloy C and (d) alloy D.

deformation, yielding followed by plastic deformation with significant work-hardening, and final shear fracture. The yield strength and work-hardening ability decrease in the order of alloys $A \Rightarrow B \Rightarrow C \Rightarrow D$. However, the compressive plasticity to failure ε_P follows an increasing order of alloys $A \Rightarrow B \Rightarrow C \Rightarrow D$, as summarized in Table 1. This is consistent with the traditional trend of the strength–plasticity relationship, i.e. improving the strength always results in a decrease in the plasticity [11].

Another common feature of the four Ti-based alloys is that the final failure always follows a shear mode, as shown in Fig. 1(a)–(d). The compressive shear fracture angle θ_C^F increases in the order of the alloys $A \Rightarrow B \Rightarrow C \Rightarrow D$. In particular, all the value of θ_C^F for the four alloys are larger than 45°, which is contrast to the previous summary [12], i.e. $0° < \theta_C^F < 45°$. This indicates that the shear fracture features of the present four alloys obviously disobey the Mohr–Coulomb criterion [4,12–14], which is suitable for the shear fracture feature of other bulk metallic glasses (BMGs) or their composites [15–18].

By SEM, the deformation morphologies of the four alloys were observed to reveal their deformation and fracture mechanism. Fig. 2(a) shows the typical deformation morphology of the Ti-based alloys after failure at a compressive plastic strain of 24%. It can be seen that dense shear bands were formed on the specimen surface, as marked by the arrow in the figure. The shear bands become bent in most areas of the specimen. For the other three alloys, similar bent shear bands are also observed (see the fractured specimens in Fig. 1). It is suggested that the bent shear bands might be caused by the high plastic flow during compression. Another deformation feature is the formation of double shear bands, and the two groups of shear bands intersect with each other, as shown in Fig. 2(b). The double shear bands are quite similar to the double-slip deformation behavior in ductile single crystals [19]. Normally, there is one group of primary shear bands, which were activated in the initial deformation stage, as marked in Fig. 2(b). With further compressive deformation, the high compressive plastic strain can also stimulate the formation of secondary shear bands, as marked in the figure. In the final failure, the shear fracture often proceeds along the primary shear band, as shown in Fig. 2(c). A strong intersection between the primary and the secondary shear bands can be clearly seen on the shear fracture plane in the figure. Therefore, it is suggested that the activation of the secondary shear bands can play three possible roles: (1) it can make a contribution to the work-hardening of the four alloys, as shown in the stress–strain curves in Fig. 1; (2) it may help to accommodate more plastic strain during compression; (3) it can contribute to the rotation of the primary shear bands.
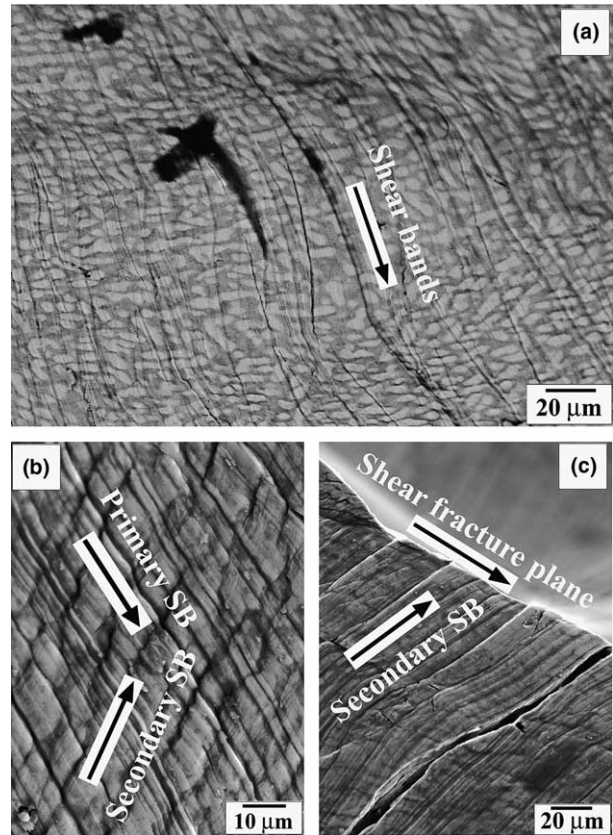
Fig. 2. (a) Formation and bending of the dense shear bands in the alloys C at a compressive plastic strain of 24%; (b) interactions of the primary shear bands with the secondary shear bands induced by the high compressive plasticity; (c) rotation of the primary shear fracture plane induced by the impingement of the secondary shear bands.
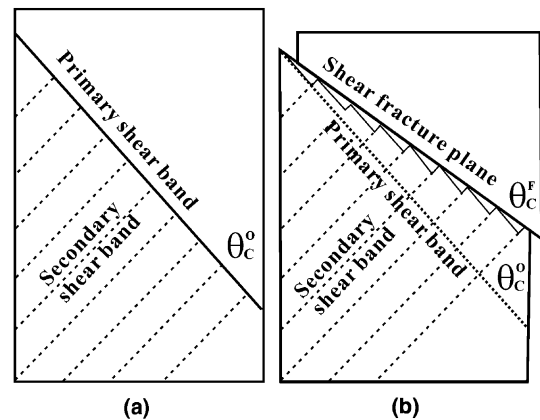
Fig. 3. (a) Illustration of interactions between primary shear bands and secondary shear bands; and (b) rotation of the primary shear plane induced by the impingement of the secondary shear bands.

For a better understanding of the relationship between the shear fracture and the rotation mechanism of the primary shear bands, the interactions of the primary and secondary shear bands can be schematically illustrated as in Fig. 3(a) and (b). We assume that

primary shear bands form in the initial deformation stage, and make an initial angle θ_C^0 with respect to the stress axis, as shown in Fig. 3(a). Then, secondary shear bands are activated due to a high compressive plastic strain, and strongly intersect with the primary shear bands. With increasing plastic strain in the specimen, strong shearing deformation will proceed along the two sets of shear bands, resulting in a strong impingement between them, as illustrated in Fig. 3(b). This strong impingement must form a shear step on one of the shear planes (see Fig. 2(c)), similar to a slip step in crystalline materials [20]. Therefore, the accumulation of dense shear steps on the primary shear plane must result in an obvious rotation of the primary shear bands towards the horizontal direction of the specimen.

From the above observations and their analysis, it is suggested that the bending or rotation of the shear bands can be attributed to the high compressive plasticity (up to 20–30%) of the Ti-based alloys. Therefore, a compressive specimen before and after deformation can be schematically illustrated as in Fig. 4(a) and (b). Assuming that the original dimension of the specimen is $a_0 \cdot a_0 \cdot l_0$, the initial shear angle of the primary shear bands is θ_C^0 and the length of the primary shear bands is l_{SB}. After being compressed to a plastic strain ε_P, its dimension is changed to $a \cdot a \cdot l$, and the angle between the primary shear plane and the stress axis is θ_C^F due to a strong rotation. Normally the volume V of the specimen and the length l_{SB} of the primary shear band remain nearly constant before and after deformation. Therefore, one can get the following relationship:

$$V = a_0 \cdot a_0 \cdot l_0 = a \cdot a \cdot l \tag{1}$$

$$l_{SB} = a_0/\sin(\theta_C^0) = a/\sin(\theta_C^F) \tag{2}$$

For a compressive specimen, the plastic strain ε_P can be expressed as:

$$\varepsilon_P = (l_0 - l)/l_0 \tag{3}$$
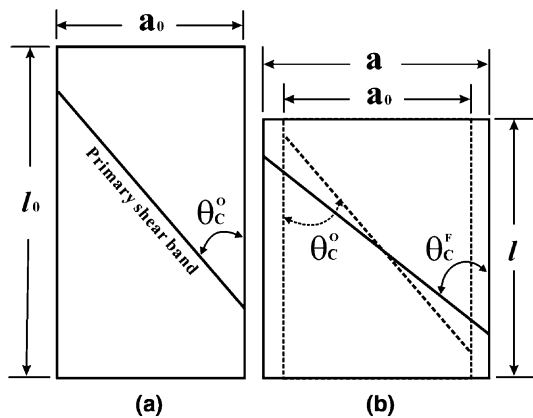
From Eqs. (1)–(3), one can get the relationship among θ_C^0, θ_C^F and the plastic strain ε_P as:

$$\sin(\theta_C^0) = \sqrt{1 - \varepsilon_P}\,\sin(\theta_C^F) \tag{4}$$

This indicates that one can approximately estimate the initial shear angle θ_C^0 of the primary shear bands if the compressive plastic strain ε_P and the final shear fracture angle θ_C^F are known. By substituting the values of ε_P and θ_C^F into Eq. (4), the calculated data of the initial shear angle θ_C^0 are obtained (Table 1). The initial shear angle θ_C^0 of the primary shear bands with respect to the stress axis is in the range 40.5–43.5° for the four Ti-based alloys. This indicates that the θ_C^0 values of the four specimens are still smaller than 45°, which is consistent with the Mohr–Coulomb criterion [4,12–14]. When taking the average value of $\theta_C^0 = 41.8 \pm 0.9°$ and Eq. (4) into account, we can extrapolate the possible final fracture angle θ_C^F, as plotted in Fig. 5. It can be seen that Eq. (4) can approximately describe the rotation mechanism of the shear fracture induced by the high compressive plasticity. Then, the difference $(\theta_C^F - \theta_C^0)$ between the two shear fracture angles before and after fracture can also be determined, as listed in Table 1. Apparently, the rotation angles $(\theta_C^F - \theta_C^0)$ increase from 2.5° to 10.5° as the compressive plastic strain is increased from 8.9% to 30%. This indicates that a high compressive plasticity can lead to a large rotation of the shear fracture plane, which is consistent with the observations in Fig. 1. However, the previously reported BMGs materials often exhibit little compressive plasticity. Accordingly, the observed final shear fracture angles are normally smaller than 45° [4,12–18]. In turn, the rotation mechanism of the shear fracture manifests itself as a decisive deformation mechanism of the nano-structured-dendrite composites, which is promising for the further development of such high-performance materials for future applications.

Fig. 4. (a) and (b) Illustration of a compressive specimen before and after deformation, and rotation of the primary shear plane.
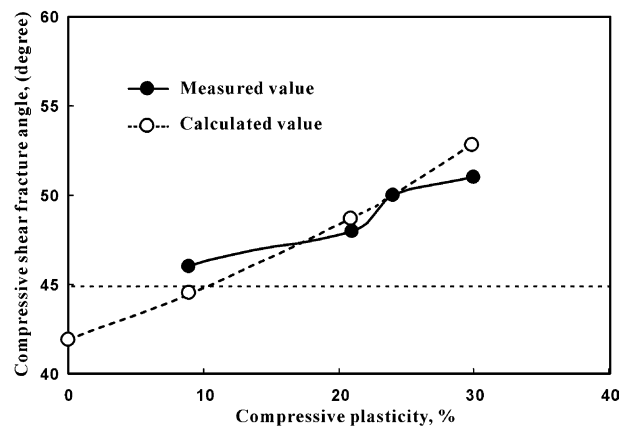
Fig. 5. Dependence of the final shear fracture angle on the applied compressive plastic strain.

4. Conclusions

Ti-based composites reinforced by ductile dendrites can exhibit very high compressive plasticity (up to 20–30%) and a strong work-hardening ability. The final shear fracture angles are often larger than 45°, which can be explained by a rotation mechanism of the primary shear bands induced by the high compressive plasticity. The rotation mechanism is caused either by bending of the primary shear bands or by strong impingement of the secondary shear bands. The rotation of the shear fracture is an obvious indication that the Ti-based composites with ductile dendrites perform well and have potential for structural applications.

Acknowledgments

References

[1] Inoue A, Zhang T, Masumoto T. Mater Trans JIM 1990;31:177.
[2] Peker A, Johnson WL. Appl Phys Lett 1993;63:2342.
[3] Argon AS. Acta Metall 1979;27:47.
[4] Donovan PE. Acta Metall 1989;37:445.
[5] Hays CC, Kim CP, Johnson WL. Phys Rev Lett 2000;84:2901.
[6] Das J, Löser W, Kühn U, Eckert J, Roy SK, Schultz L. Appl Phys Lett 2003;82:4690.
[7] He G, Eckert J, Löser W, Schultz L. Nature Mater 2003;2:33.
[8] He G, Löser W, Eckert J. Acta Mater 2003;51:5223.
[9] He G, Eckert J, Löser W, Hagiwara M. Acta Mater 2004;52:3035.
[10] He G, Eckert J, Dai QL, Sui ML, Löser W, Hagiwara M, et al. Biomaterials 2004;24:5115.
[11] Sandor BI, editor. Strength of materials. Englewood Cliffs New Jersey: Prentice Hall, Inc; 1978. p. 07632.
[12] Zhang ZF, He G, Eckert J, Schultz L. Phys Rev Lett 2003;91:04550501.
[13] Lund AC, Schuh CA. Acta Mater 2003;51:5399.
[14] Lund AC, Schuh CA. Intermetallics 2004;12:1159.
[15] Wright WJ, Saha R, Nix WD. Mater Trans 2001;42:642.
[16] Lewandowski JJ, Lowhaphandu P. Philos Mag 2002;82:3427.
[17] Zhang ZF, Eckert J, Schultz L. Acta Mater 2003;51:1167.
[18] Zhang ZF, Eckert J, Schultz L. Metall Mater Trans 2004;A35:3489.
[19] Reid CN, editor. Deformation geometry for materials scientists. Pergamon Press; 1973.
[20] Honeycombe RWK, editor. The plastic deformation of metals. Edward Amold, London: Cambridge University Press; 1984.